Controls on Primary Productivity in the Eastern Equatorial Pacific, East of the Galapagos Islands, During the Penultimate Deglaciation

Lucía Quirós-Collazos[1], Eva Calvo[1], Stefan Schouten[2,3], Marcel T. J. van der Meer[2], Marta Rodrigo-Gámiz[4], Leopoldo D. Pena[5], Isabel Cacho[5], and Carles Pelejero[1,6]

[1]Institut de Ciències del Mar, CSIC, Barcelona, Spain, [2]Department of Marine Microbiology and Biogeochemistry, NIOZ Royal Netherlands Institute for Sea Research and Utrecht University, Texel, The Netherlands, [3]Department of Earth Sciences, Organic Geochemistry, Utrecht University, Utrecht, The Netherlands, [4]Department of Stratigraphy and Paleontology, Universidad de Granada, Granada, Spain, [5]Department of Earth and Ocean Dynamics, Universitat de Barcelona, Barcelona, Spain, [6]Institució Catalana de Recerca i Estudis Avançats, Barcelona, Spain

Abstract Modern biogeochemical conditions of the Eastern Equatorial Pacific (EEP) region are characterized by high macronutrient concentrations but low phytoplankton abundance due to both iron and silicic acid limitation. Since primary producers significantly impact the global carbon cycle, paleoproductivity in relation to climate change and nutrient availability in this region has been a topic of a number of studies. However, the complex dynamics of this region, especially east of the Galapagos Islands, has led to some discrepancies when linking reconstructed paleoproductivity with potential mechanisms for higher primary productivity. Here we focus on reconstructing primary productivity of haptophyte algae and diatoms, as well as continental material input, sea surface salinity, and sea surface temperature, and compare these reconstructions with existing records for the period comprised between 150 and 110 ka (the penultimate deglaciation period) with the aim to understand the mechanisms that most significantly influence phytoplankton growth over the EEP region east of the Galapagos Islands. Our results suggest enhanced upwelling in the EEP system during the penultimate deglaciation and increased phytoplankton abundance mainly as the result of both the increasing influence of nutrient-rich Southern Ocean sourced waters through the Equatorial Undercurrent and a higher input of iron through atmospheric deposition. The highest phytoplankton abundances recorded at the study site during the penultimate deglaciation also suggest that maximum input of nutrients might have occurred during the millennial-scale event Heinrich Event 11 in the North Atlantic as a result of global atmospheric and oceanic reorganizations.

1. Introduction

Oceanic primary producers play a determinant role in global biogeochemical cycles. In this regard, marine phytoplankton represents a key element of the global carbon cycle since it is a main driver for the transfer of CO_2 from the atmosphere to the deep ocean and thus exerts an important control on global climate (Sigman & Boyle, 2000). Due to the strong impact that phytoplankton growth can have on the carbon cycle, both at short and long time scales, improving the knowledge on the biogeochemical processes and feedbacks involved in primary productivity (PP) at different space and time scales is an important aspect to understand how the Earth's system will respond to the current global climate change.

An interesting region to study past changes and dynamics in PP is the Eastern Equatorial Pacific (EEP) (Figure 1) because it is affected by one of the largest upwelling zones in the world, the Equatorial Pacific Cold Tongue, that today acts as a major ocean-to-atmosphere CO_2 source (Graham & White, 1988; Takahashi et al., 2009). This upwelling area is a low-silicate, high-nutrient, low-chlorophyll region and is characterized by high nitrogen and phosphorus concentrations but low phytoplankton abundance due to both iron and silicic acid limitation (Brzezinski et al., 2011; Dugdale et al., 1995). Therefore, changes in biogeochemical properties and different nutrient availability can affect the phytoplankton community composition in this region and, thus, its impact on the carbon cycle (Brzezinski et al., 2011; Chavez, 1999; Gómez et al., 2007; Watkins et al., 1998).
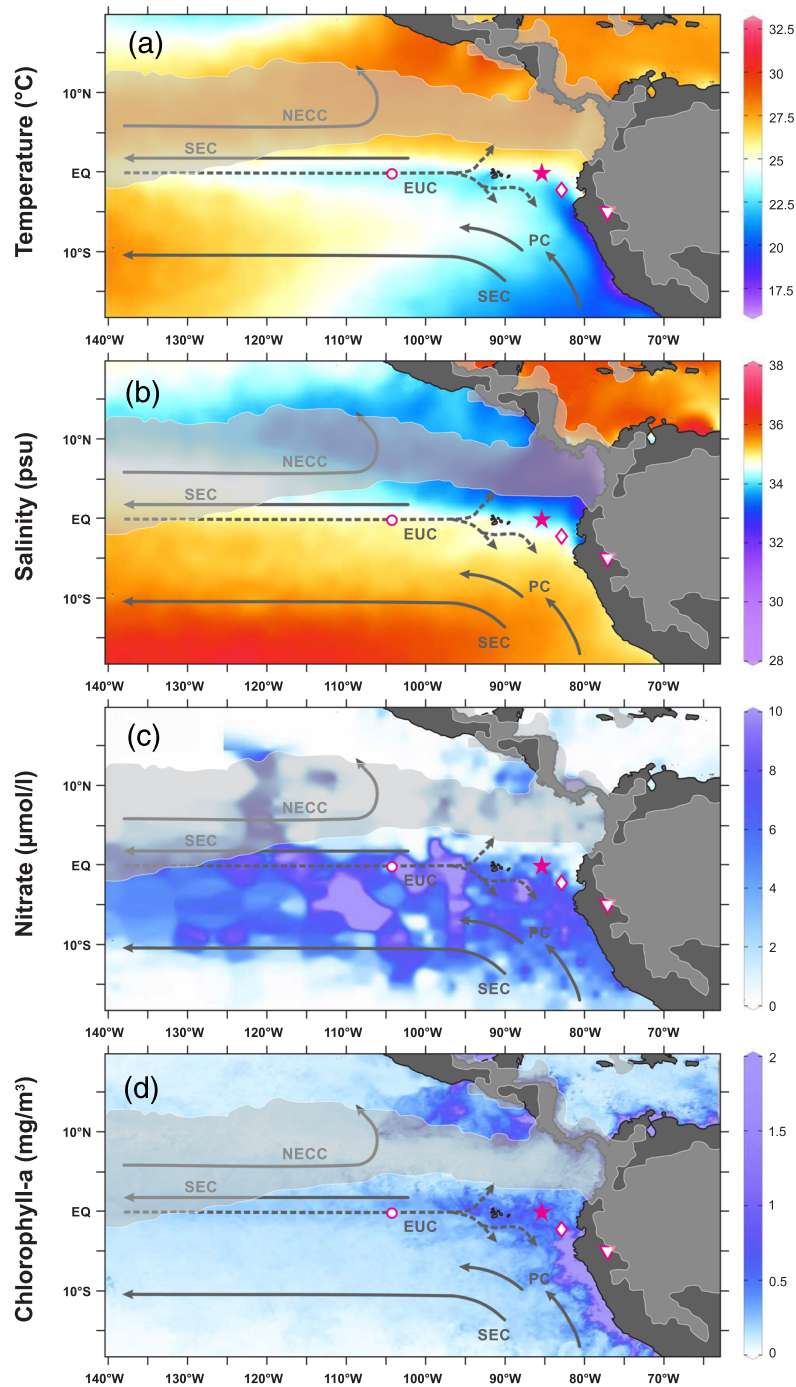
Figure 1. Modern sea surface temperature, salinity, nitrate, and chlorophyll-a distributions in the EEP. The three upper panels show long term annual mean sea surface (a) temperature (Locarnini et al., 2013), (b) salinity (Zweng et al., 2013), and (c) nitrate (Garcia et al., 2014) (from the World Ocean Atlas 2013, https://www.nodc.noaa.gov/OC5/woa13/woa13data.html) and the lower panel shows (d) chlorophyll-a distribution during August 2016 as an example of phytoplankton abundance during the summer season, when the EEP upwelling system is stronger (data from MODIS [Moderate Resolution Imaging Spectroradiometer] on the Aqua NASA's satellite). In order to highlight the modern mean annual ITCZ position, the gray shaded area shows the region with precipitation rates higher than 6.0 mm per day (Legates & Willmott, 1990). ODP Site 1240 is highlighted with a pink star; the nearby cores and speleothem used in the discussion are depicted with an empty pink circle (ODP 849), diamond (V19-30) and inverted triangle (Cueva del Diamante), respectively. The main surface (solid dark gray arrows) and subsurface (dashed dark gray arrows) currents are indicated: North Equatorial Countercurrent (NECC), South Equatorial Current (SEC), Equatorial Undercurrent (EUC), and Peruvian Current (PC).

PP reconstructions performed all along the Equatorial Pacific have shown both spatial (Costa et al., 2017 and references therein) and temporal (Winckler et al., 2016) variability over the last glacial cycles, pointing to different processes to explain the regional patterns of observed PP. The variable availability of the limiting micronutrient Fe and/or the macronutrient Si could explain this variability in PP (Calvo et al., 2011; Loveley et al., 2017; S. S. Kienast et al., 2013; Winckler et al., 2016). However, in this region, it is still controversial whether past PP was enhanced because of iron fertilization from eolian dust or through upwelling of the Equatorial Undercurrent (EUC) (Badejo et al., 2017; Jacobel et al., 2019; Loubere, 2000; Loveley et al., 2017; Marcantonio et al., 2019; Winckler et al., 2016). Studies carried out along the equator, from the Central Pacific to the Galapagos Islands, concluded that most of the iron was delivered from the upwelled waters of the EUC, since the amount of eolian dust arriving to that region west of the Galapagos Islands was various orders of magnitude lower than the iron supplied by the EUC (Costa et al., 2016; Winckler et al., 2016). However, similar studies in the easternmost EEP, east of the Galapagos Islands, suggested continental dust as a significant iron source, which seems reasonable given the proximity to the continent (Calvo et al., 2011; Loveley et al., 2017; Marcantonio et al., 2019; S. S. Kienast et al., 2013).

In order to shed some light on the processes affecting PP east of the Galapagos Islands, various studies have focused on the last deglaciation, when ice sheets rapidly withdrew in concert with a rise in atmospheric CO_2, global temperatures, and sea level (Cheng et al., 2009; Marcott et al., 2014; Shakun et al., 2012). In this region, and for this particular time interval, several studies reported an increase in export production (Bradtmiller et al., 2006; Calvo et al., 2011; Dubois et al., 2010; M. Kienast et al., 2006; S. S. Kienast et al., 2007). Data on surface nutrient consumption pointed towards an increase of nutrient availability fueling the increase in PP (Dubois et al., 2011; Robinson et al., 2009), which was attributed to the influence of nutrients sourced from the Southern Ocean that are delivered to the EEP through intermediate waters (Sarmiento et al., 2004). High-resolution records showed that these processes were especially relevant during the time when millennial-scale cold events, Heinrich Event (HE) 1 and the Younger Dryas, developed in the North Atlantic (Anderson et al., 2009; S. S. Kienast et al., 2006, 2013). In this regard, a relative increase of diatoms over coccolitophores at the EEP during HE1 and the Younger Dryas was attributed to the arrival of Si-rich waters from the Southern Ocean associated with the increase in deep water ventilation at those high-latitude regions (Calvo et al., 2011). In addition, [232]Th flux data indicated increasing dust inputs during HE1 and the Younger Dryas east of the Galapagos Islands (S. S. Kienast et al., 2013) related to changes in the global wind regime (Leduc et al., 2007), thus suggesting that the region was iron-fertilized by eolian dust enhancing export PP (S. S. Kienast et al., 2013).

With the aim to broaden the knowledge on the controlling factors in PP dynamics at the easternmost region of the EEP, here we explore the penultimate deglaciation, a time interval less studied through high-resolution records than the last deglaciation. In this study, we have reconstructed diatom and haptophyte export production from a core located east of the Galapagos Islands during the period from 150 to 110 ka cal BP. Down core marine sediment samples from ODP Site 1240 have been used for the analysis of C_{28} and C_{30} 1,14-diols, $C_{37:2}$ and $C_{37:3}$ long chain ketones (alkenones), and 24-methylcholesta-5,22-dien-3β-ol (brassicasterol) as proxies of PP. Alkenones were also used to infer past sea surface temperatures (SST). In addition, n-alkanes and stable isotope ratios in C_{37} alkenones (δD_{C37}) were analyzed to obtain further environmental information on the input of continental material and relative salinity changes, respectively. Our results are compared with previously published data from the same ODP Site 1240 core (Pena et al., 2008) and from other nearby cores to better understand the mechanisms controlling PP changes during the penultimate glacial/interglacial transition in the study region.

2. Regional Setting

ODP Site 1240 (0°01.31′N, 86°27.76′W, Ocean Drilling Program, Leg 202), in the easternmost part of the EEP, was retrieved from 2,921 m water depth in the Panama Basin (Figure 1). Oceanic surface conditions are shaped by the presence of northeasterly and southeasterly trade winds which come together in the Intertropical Convergence Zone (ITCZ). The ITCZ is defined by the region where northeast and southeast trade winds converge and maximum precipitation rates are recorded (Philander et al., 1996; Schneider et al., 2014; Waliser & Gautier, 1993). It plays an important role on global climate by transferring heat from the tropics to the poles and by driving and setting the distribution of global precipitation patterns like

monsoon rains (Schneider et al., 2014). As a result of Ekman transport, wind-driven dynamics in the EEP result in two different sea surface conditions divided by the equatorial front (EF): a region south of the EF where divergent surface circulation favors the upwelling of cooler and saltier subsurface waters of the EUC and a region north of the EF where convergent surface circulation results in warmer SSTs known as the Eastern Pacific Warm Pool (Fiedler & Talley, 2006). In this regard, ODP Site 1240 is likely to be sensitive to changes in these surface circulation systems since it is located under the modern northern boundary of the Equatorial Pacific Cold Tongue (Figure 1) but also to changes in the upwelling and the characteristics of the EUC water mass. The influence of the EUC east of the Galapagos Islands has been detected by several studies based on hydrographic data (Fiedler & Talley, 2006; Kessler, 2006; Lukas, 1986; Toggweiler et al., 1991; Tsuchiya et al., 1989) but also through the ε_{Nd} water-mass tracer measured at the study site after comparison with the ε_{Nd} value from the EUC at the Central Equatorial Pacific (Pena et al., 2013).

The ITCZ-EF linkage and its influence over the EEP upwelling system also determine the existence of different PP regimes across the region by regulating the supply of nutrient-rich subsurface waters to the euphotic zone (Fiedler et al., 1991; Pennington et al., 2006; Rincón-Martínez et al., 2011): North of the EF, stratification and oligotrophic conditions are dominant (with the exception of the Costa Rica Dome and the Panama Bight, favored by local wind-driven coastal upwelling), while south of the EF, the upwelling of EUC waters from Southern Ocean origin dominate average conditions.

Precipitation, wind, and oceanic patterns in the EEP, as well as changes in the biogeochemical composition of surface and subsurface waters, are affected by changes in northern and southern high latitudes. For instance, changes in North Atlantic temperatures can significantly affect the strength of the northeasterly trade winds and trigger latitudinal migrations of the ITCZ rain belt, thus affecting precipitation, wind, and surface circulation patterns in the EEP (Dubois et al., 2014; Leduc et al., 2007). Furthermore, oceanic teleconnections occur through EUC subsurface waters, which are formed in the western equatorial Pacific as a result of mixing of local water masses with a major proportion of Antarctic Intermediate Water (AAIW), Subantarctic Mode Water (SAMW), and some influence of North Pacific Intermediate Water and flow eastward along the equator (Bostock et al., 2010; Leduc et al., 2010; Lukas, 1986; Rippert et al., 2017; Tsuchiya, 1981; Tsuchiya et al., 1989). The AAIW and SAMW geochemical properties and nutrient content that these water masses acquire at their high-latitude formation region have been found to be transferred as far as east of the Galapagos Islands, through the EUC water mass (Bostock et al., 2010; Dubois et al., 2011; Pena et al., 2013), eventually modulating the composition and growth of the local biological community (Calvo et al., 2011; Povea et al., 2016; Timmermann et al., 2007).

3. Methodology

In this study, down core marine sediment samples from ODP Site 1240 (Figure 1) have been analyzed in order to obtain estimates of export primary production, input of continental material, SST, and relative changes in surface salinity for the period between 150 and 110 ka. For a broader context, comparisons with data from nearby cores ODP 849 (Winckler et al., 2008) and V19-30 (Hayes et al., 2011) (Figure 1), and also from the North Atlantic (ODP Site 980; Govin et al., 2012; Irvalı et al., 2016), the West Equatorial Pacific (Borneo Cave; Carolin et al., 2016), and the Southwest Pacific (MD97-2120; Pahnke & Zahn, 2005), are also included to elucidate potential linkages between high and low latitudes variability.

The age model of the core section presented in this study (sediment depth from ~13 to 17 m) is based on Rippert et al. (2017), where combined $\delta^{18}O$ records from the benthic foraminifera *Cibicidoides wuellerstorfi* and the deep-dwelling planktonic foraminifera *Globorotaloides hexagonus* of ODP Site 1240 were aligned graphically to the global benthic $\delta^{18}O$ stack LR04 (Lisiecki & Raymo, 2005). This age model provides sedimentation rates of 4.6–17.8 cm ka^{-1} for the studied period which, considering the sampling resolution for biomarkers (every 4 or 8 cm), corresponds to an average time resolution of ~400 years per sample. Comparisons drawn with the above-mentioned climate records have been performed using the original chronologies published by each record, assuming thus the limitations and age uncertainties associated with the lack of absolute age constraints.

3.1. Molecular Biomarkers

Molecular biomarkers from the total lipid extracts obtained from 96 marine sediment samples were analyzed following methods in Villanueva et al. (1997) and Pelejero et al. (1997). Briefly, freeze-dried marine sediment samples were homogenized and soaked in dichloromethane (DCM) to extract the organic substances using an ultrasonic water bath, after addition of *n*-hexatriacontane, used as an internal standard for compound quantification. Alkaline hydrolysis, with a potassium hydroxide solution in methanol (6%), and polar compound derivatization with N,O-Bis(trimethylsilyl)trifluoroacetamide (BSTFA) were carried out to break ester bonds prior to analyses by gas chromatography (GC).

Compounds of interest were di- and tri-unsaturated C_{37} alkenones ($C_{37:2}$ and $C_{37:3}$), 24-methylcholesta-5,22-dien-3β-ol (brassicasterol), and *n*-alkanes. The lipid extracts were analyzed using an Agilent 7890 Gas Chromatograph with a flame ionization detector (GC-FID) equipped with an HP1 fused silica capillary column (60 m × 0.25 mm, film thickness 0.25 μm) and using hydrogen as carrier gas. The GC temperature program started with a 20 °C/min ramp from 90 °C to 190 °C, followed by a 6 °C/min ramp to 295 °C (holding time of 49 min) and a final ramp of 10 °C/min to 310 °C (holding time of 10 min).

$C_{37:2}$ and $C_{37:3}$ alkenones are compounds synthesized by haptophyte algae, which preferentially dwell in the photic zone of the ocean (Volkman et al., 1980). These marine photosynthetic organisms are widely spread in all ocean basins, and the relative abundance of C_{37} alkenones, as defined by the unsaturation index $U^{K'}_{37}$ (Prahl & Wakeham, 1987), has been widely used as an SST proxy. In order to derive SST values, we use the global surface sediment calibration equation from Conte et al. (2006) which, although virtually identical to that from Müller et al. (1998), is based on a larger compilation of core tops. Moreover, a previous study performing a regional calibration of $U^{K'}_{37}$ vs SSTs in surface sediments over the EEP (M. Kienast et al., 2012) found the regional calibration not being statistically different (95% confidence level) from the existing global calibration equations of Müller et al. (1998) and Conte et al. (2006). With the Conte et al. (2006) calibration, the ODP Site 1240 core-top estimate provides an SST of 24.3 °C, which is in good agreement (within the calibration error range, ±1.1 °C) with the modern surface annual mean of 24.7 °C at this location (Locarnini et al., 2013). In addition, concentrations of long chain alkenones (in units of microgram per gram of dry sediment, as hereafter will be referred all the analyzed biomarker concentrations) can also provide information on past haptophyte export production (Brassell, 1993; Calvo et al., 2004, 2011; Martínez-Garcia et al., 2009; Villanueva et al., 2001).

Brassicasterol is the most abundant sterol in pennate diatoms (Rampen et al., 2010; Volkman, 2003) and can be used as a diatom proxy (e.g., Calvo et al., 2011; Werne et al., 2000). However, other microalgae like haptophytes also synthesize this compound (Volkman et al., 1981) and, thus, when comparing C_{37} alkenones and brassicasterol records, it is critical to focus on periods when these records are decoupled, which would imply that the biological sources of these biomarkers were different.

Long chain *n*-alkanes with an odd number of carbon atoms are found in the waxes of higher plant tissues (Eglinton & Hamilton, 1967; Eglinton & Eglinton, 2008) and are transported to the ocean by wind or rivers (Gagosian et al., 1987), so these compounds have commonly been used as a continental material and dust input proxy (Calvo et al., 2004, 2011; Lamy et al., 2014; Martínez-Garcia et al., 2009, 2011). In the ODP Site 1240 location, 600 km away from the continent, eolian dust input represents the main source of land-originated particles (Singh et al., 2011). Here, we only present data from the C_{29} *n*-alkane homolog, as it was the most abundant *n*-alkane (the distribution of these compounds had a strong odd to even preference, and the C_{29} *n*-alkane showed the same trend as the total *n*-alkane abundance).

Other analyzed molecular biomarkers were the C_{28} and C_{30} 1,14-long chain alkyl diols (hereafter referred to as diols), which are produced by centric diatoms belonging to the genus *Proboscia* (Rampen et al., 2008; Sinninghe Damsté et al., 2003). No other biological source is known for these specific compounds apart from the marine heterokont algae *Apedinella radians*, a microalgae which is predominant in estuarine and brackish environments (Rampen et al., 2011). Given the location of ODP Site 1240, we are confident that the major source for the C_{28} and C_{30} 1,14-diols were *Proboscia* diatoms and, thus, these diols can be used as a proxy for *Proboscia* diatom export production. The C_{28} and C_{30} 1,14-diols were analyzed at the NIOZ Royal Netherlands Institute for Sea Research using a smaller set of the original lipid extracts (resulting in a lower resolution record), which were separated into nonpolar and polar fractions and analyzed with

chromatographic techniques following Sinninghe Damsté et al. (2003). Briefly, these fractions were obtained using a glass pipette column filled with activated Al_2O_3, and the lipid extracts were eluted with hexane/DCM (9:1, v:v) to obtain the nonpolar fractions and with DCM/MeOH (1:1, v:v) for the polar ones, after the addition of two internal standards to allow quantification, that is, a deuterated ante-iso C_{22}-alkane and C_{22} 7,16-diol. Diols analyses were performed on the polar fraction which were compound-derivatized with BSTFA and pyridine. These fractions were analyzed using gas chromatography-mass spectrometry (GC-MS) with a CP-Sil 5 CB capillary column (25 m × 0.32 mm, film thickness 0.12 μm) and using helium as the carrier gas. The GC temperature program started with a 20°C/min ramp from 70°C to 130°C, followed by a 4°C/min ramp to 320°C, with a holding time of 25 min. The long-chain diols were quantified using selected ion monitoring (SIM) of the masses 299 and 327.

3.2. Stable Hydrogen Isotopes of C_{37} Alkenones

Analyses of the stable hydrogen isotopic ratio of C_{37} alkenones (hereafter δD_{C37}) were also performed at the NIOZ Royal Netherlands Institute for Sea Research. Two batches, a test batch and the bulk of the samples, of total lipid extracts were separated into three fractions over Al_2O_3 columns using hexane/DCM 9:1 (v:v) to elute the apolar fraction, hexane/DCM 1:1 (v:v) to elute the ketone (alkenone) fraction, and DCM/MeOH 1:1 (v:v) to elute the polar fraction. Ketone fractions were analyzed using a GC-FID to determine alkenone concentrations prior to running them on a GC thermal conversion isotope ratio monitoring mass spectrometer (GC/TC/irMS; Thermo Scientific TRACE 1310 coupled to a Thermo Scientific Delta V™) to measure compound specific hydrogen isotope ratios. Both the GC-FID and the GC/TC/irMS were equipped with an Agilent CP-Sil 5 column (25 m × 0.32 mm internal diameter; film thickness 0.12 μm for the GC-FID and 0.4 μm for the GC/TC/irMS analyses). GC temperature programs were the same as discussed in M'boule et al. (2014). The H_3^+ factor was measured daily on the GC/TC/irMS prior to running the samples and was 4.2 ± 0.1 ppm mV^{-1} for both batches. A Mix B standard (supplied by A. Schimmelmann, Indiana University) was analyzed daily to assess machine accuracy, and samples were only analyzed when measured standard values deviated on average by less than 5‰ from the known values and the standard deviation for these offsets was also less than 5‰. Samples were measured at least in duplicate, and squalane was coinjected with each analytical run as internal control. The average value for squalane for both sample batches was −166.5‰ with a standard deviation of 4.8‰. This compares well with the known isotope value for squalene, −170‰, determined by TC elemental analysis irMS. All C_{37} alkenone peaks were integrated as a single peak and values are, therefore, reported as the combined values of the $C_{37:2}$ and $C_{37:3}$ alkenones (van der Meer et al., 2013).

The analyses of δD_{C37} have been successfully used as a qualitative tracer of changes in water salinity (Kasper et al., 2014; Pahnke et al., 2007; Weiss et al., 2019a). Water stable hydrogen isotopic composition (δD) is mainly conditioned by isotopic fractionation occurring during the condensation and evaporation processes that take place within the water cycle (Gat, 1996). The strong correlation ($R^2 > 0.99$) found between δD_{C37} and δD values of the water in which the alkenones were produced makes the δD_{C37} a reliable proxy to trace relative changes in surface seawater salinity (Englebrecht & Sachs, 2005). A factor that could affect D/H fractionation, in addition to salinity, is a change in species relative abundance (δD_{C37} values in *Emiliania huxleyi* batch cultures where found to be ~30‰ higher than those from *Gephyrocapsa oceanica*, Schouten et al., 2006); however, no major changes in species composition were detected in our study site and period (López-Otálvaro et al., 2008 and personal communication).

In order to obtain information on relative local salinity changes, the δD_{local} parameter was inferred after subtraction of the global sea level component from the δD_{C37} record. To do so, we first converted the sea level $\delta^{18}O$ curve ($\delta^{18}O_{s.l.}$) from Waelbroeck et al. (2002) into $\delta D_{s.l.}$ values using the Rozanski et al. (1993) equation:

$$\delta D_{s.l.} = \delta^{18}O_{s.l.} \times 8.13 + 10.8.$$

The $\delta D_{s.l.}$ uncertainty is ±1.22‰, which was calculated from the $\delta^{18}O_{s.l.}$ uncertainty (Waelbroeck et al., 2002) through error propagation. Then, the relative local salinity proxy was obtained through the expression

$$\delta D_{local} = \delta D_{C37} - \delta D_{s.l.}.$$

For the estimation of each δD_{local} data point uncertainty, the sum of each standard deviation plus the $\delta D_{s.l.}$ uncertainty was calculated. The average uncertainty for the δD_{local} dataset is $\pm 3\text{‰}$.

3.3. Seawater Stable Oxygen Isotopic Composition ($\delta^{18}O_{sw}$)

In order to obtain an additional indicator of relative local sea surface paleosalinity changes, the seawater $\delta^{18}O$ record is presented in this study based on the analysis of stable oxygen isotopes ($\delta^{18}O_c$) and Mg/Ca ratio in foraminifera shells of *Globigerinoides ruber*, previously published by Pena et al. (2008). The $\delta^{18}O_{sw}$ composition was obtained by subtraction of the global sea level component ($\delta^{18}O_{s.l.}$; Waelbroeck et al., 2002) and the Mg/Ca derived temperature ($SST_{Mg/Ca}$; Pena et al., 2008) from the *G. ruber*-$\delta^{18}O_c$ record using the equation from Bemis et al. (1998):

$$\delta = \delta^{18}O_c - \delta^{18}O_{s.l.} - \left((SST_{Mg/Ca} - 16.5)/(-4.8) \right).$$

Lastly, the δ parameter was converted from V-PDB to V-SMOW standard using the following expression:

$$\delta^{18}O_{sw} = (\delta + 0.27)/0.99973.$$

We estimated the total $\delta^{18}O_{sw}$ uncertainty to be $\pm 0.49\text{‰}$ (note that the $\delta^{18}O_{s.l.}$ uncertainty is $\pm 0.15\text{‰}$).

4. Results

4.1. Biomarkers Concentrations

The concentrations of long-chain alkenones (Figure 2f), brassicasterol, and $C_{28} + C_{30}$ 1,14-diols (Figure 2g) are used here to provide information on how export production changed across the penultimate deglaciation, most likely linked to changes in haptophyte algae and diatom productivity. ^{230}Th-normalized fluxes would more accurately represent the vertical fluxes of these compounds through the water column to deep sea sediments but, unfortunately, there are no ^{230}Th measurements available from ODP Site 1240 during the penultimate deglaciation. However, comparison between biomarkers concentrations and ^{230}Th-derived fluxes in younger sections of the companion core ME0005-24JC (Dubois et al., 2010) shows a strong correlation between the two ($R^2 = 0.78$ for alkenones and $R^2 = 0.79$ for the C_{29} *n*-alkane). Thus, we assume that, at this location, the concentrations of the studied molecular biomarkers are good recorders of their fluxes to the sediments and, regarding the marine proxies, they mostly represent changes in export production/marine productivity. In addition, the good agreement with other export production proxies, such as opal fluxes (Figure 2g), provides additional support for the use of concentrations of marine lipids as export production proxies at our site.

In our record, the concentration of all three biomarkers increased between 140 and 128 ka in two steps. The most significant change occurred during the second half of the deglaciation, when haptophytes and diatoms export production sharply increased to reach maximum values (28, 1.8, and 26 µg/g for C_{37} alkenones, brassicasterol, and $C_{28}+C_{30}$ 1,14-diols, respectively) between 133 and 130 ka. While C_{37} alkenone concentrations rapidly decreased before 130 ka, diatom proxies still showed sustained high values at that time. In addition, brassicasterol and $C_{28} + C_{30}$ 1,14-diols showed a larger late versus early deglaciation relative increase than C_{37} alkenones, suggesting that the diatoms' contribution to total productivity was probably higher than that from haptophytes between 133 and 125 ka (Figure 2f, g). Although brassicasterol might be synthesized by both phytoplankton communities, the consistent large increase showed by the *Proboscia* proxy during the last half of the deglaciation and the brassicasterol decoupling with the alkenones record after 130 ka point toward a significant contribution of diatoms at this time.

The concentration of the C_{29} *n*-alkane increased between 140 and 128 ka (Figure 2f), similar to the trend observed in the phytoplankton export production proxies, following a two-step increase with maximum concentrations (up to 0.4 µg/g) between 131 and 129 ka.
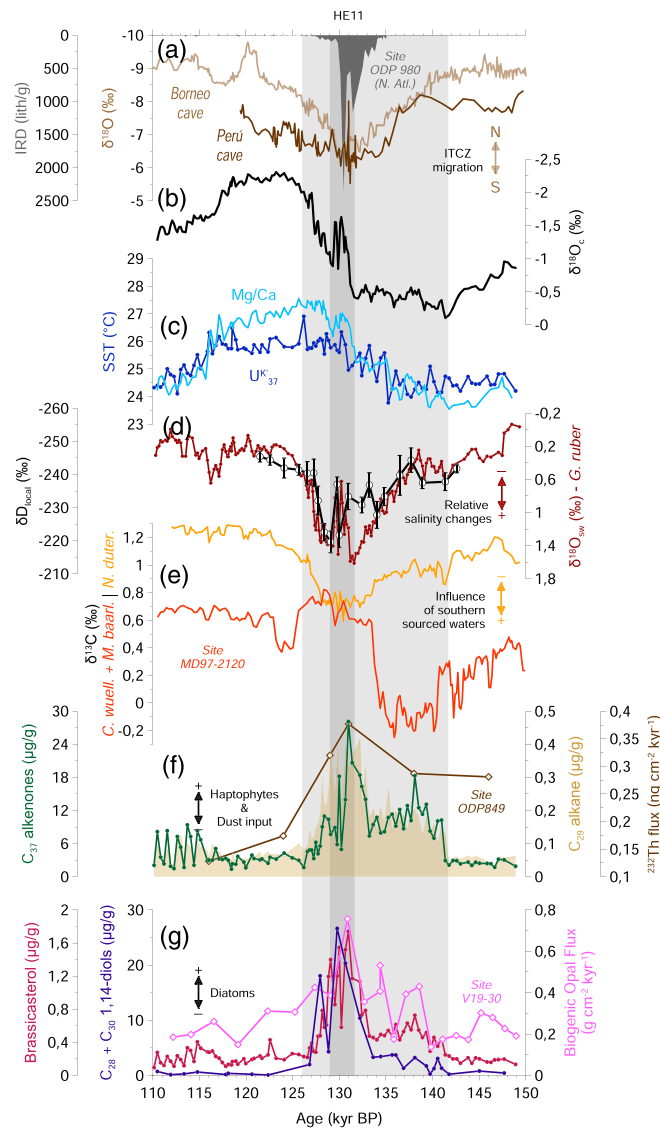
Figure 2. Multiproxy records from ODP Site 1240 spanning the period between 150 and 110 ka and their comparison with other available climate records. (a) IRD record from the North Atlantic core ODP 980 (gray-filled curve, Irvalı et al., 2016), as a proxy of HE11 occurrence, and ice-volume corrected stalagmite $\delta^{18}O$ composite record from Clearwater cave in Borneo (light brown curve, Carolin et al., 2016, and references therein) and Cueva del Diamante cave in Perú (dark brown curve, see Figure 1 for location, Cheng et al., 2013; Cueva del Diamante record has been corrected for $\delta^{18}O$ ice volume effect using the mean ocean $\delta^{18}O$ curve of Waelbroeck et al. (2002)) as proxies of ITCZ latitudinal migrations. (b) Planktonic foraminifera *G. ruber*-$\delta^{18}O_c$ referred to the V-PDB scale (black curve, Pena et al., 2008) for stratigraphic reference. (c) $U^{K'}_{37}$ (dark blue curve, this study) and planktonic foraminifera *G. ruber*-Mg/Ca (light blue curve, Pena et al., 2008) derived SSTs. (d) $\delta^{18}O_{sw}$ of surface foraminifera *G. ruber* (dark red curve, this study) and sea level corrected values of δD_{C37} (that is, δD_{local}) measured in alkenones (white dots-black line curve, this study) as proxies of relative change in local sea surface salinity. (e) $\delta^{13}C$ of thermocline-dwelling foraminifera *Neogloboquadrina dutertrei* (yellow curve, Pena et al., 2008) as a proxy of the influence of Southern Ocean-sourced water to the EEP and $\delta^{13}C$ of combined benthic foraminifer species *Cibicidoides wuellerstorfi* and *Melonis barleeanum* from the eastern New Zealand sector core MD97-2120 (dark orange curve, Pahnke & Zahn, 2005). (f) Concentrations of the marine biomarker C_{37} alkenones (dark green curve, this study) and terrestrial biomarker C_{29} *n*-alkane (gold filled curve, this study) as proxies of haptophyte algae export production and dust inputs, respectively; ^{232}Th flux from EEP core ODP 849 as a proxy of eolian dust flux (dark brown curve, see Figure 1 for location, Winckler et al., 2008). (g) Concentrations of marine biomarkers $C_{28}+C_{30}$ 1,14-diols (purple curve, this study) and brassicasterol (dark pink curve, this study) and biogenic opal fluxes from the nearby core V19-30 (light pink curve, see Figure 1 for location, Hayes et al., 2011) as proxies for *Proboscia* diatoms and 'diatoms + haptophytes' export production and organic silica flux, respectively. Lighter and darker gray shaded vertical bars mark the deglaciation and HE11 time intervals, respectively, according to the $\delta^{18}O_c$ chronostratigraphic curve of ODP Site 1240.

4.2. Surface Seawater Properties

The temperature evolution between 150 and 110 ka was evaluated using the alkenone unsaturation index, $U_{37}^{K'}$ (Figure 2c) and the Mg/Ca ratio from the planktonic foraminifera *G. ruber* (Pena et al., 2008). The $U_{37}^{K'}$-SST recorded a warming trend during the deglaciation with an average change over the deglaciation of 1.5°C, based on the difference between glacial (147 to 138 ka) and interglacial (128 to 122 ka) temperatures. During the penultimate glacial maximum, $U_{37}^{K'}$-SST was up to 0.75°C warmer than Mg/Ca-SST, while both proxies mostly agreed during the first half of the deglaciation.

Two independent indicators of relative changes in local surface salinity were also considered. On one hand, we inferred the $\delta^{18}O_{sw}$ composition by correcting the *G. ruber*-$\delta^{18}O_c$ record for the Mg/Ca-derived temperature and the global sea level component (Waelbroeck et al., 2002). On the other hand, we measured δD_{C37} and also removed the global sea level effect, obtaining the δD_{local} (Figure 2d). In order to translate salinity changes into practical salinity units (psu), some calibration equations have been developed for the δD_{C37}-salinity relationships using culture experiments (M'boule et al., 2014; Schouten et al., 2006) and marine surface and sediment surface samples (Gould et al., 2019; Weiss et al., 2019b). However, recent paleosalinity reconstructions from the Chile margin found strong discrepancies among the paleosalinity curves obtained after applying those different calibration equations, suggesting that modern observed sensitivity of δD_{C37} ratios to salinity might have been different during past time periods (Weiss et al., 2019a). For the $\delta^{18}O_{sw}$ data, Benway and Mix (2004) proposed a $\delta^{18}O_{sw}$-salinity relationship for the Panama Basin region based on modern climatology. Since this relationship is highly dependent on local and global hydrological conditions, there is no guarantee that the $\delta^{18}O_{sw}$-salinity relationship is held over long time periods as the one studied here. Therefore, for the study period, changes in relative local surface salinity have been assessed only qualitatively through the use of relative changes in the δD_{local} and $\delta^{18}O_{sw}$ proxies. The coefficient of correlation (R^2) of 0.64 between these two independent parameters provides additional confidence in using these proxies as relative salinity change indicators.

As a general trend, the penultimate deglaciation was characterized by a significant increase in the $\delta^{18}O_{sw}$ of ~1.3‰ relative to the glacial and interglacial values, when $\delta^{18}O_{sw}$ showed similar values of ~0.1‰. From 132 to 129 ka, however, the $\delta^{18}O_{sw}$ exhibited a rapid and brief decrease of about 0.8‰, indicating a relative decrease in salinity. Regarding the δD_{local} record, there was an increasing trend of ~14‰ throughout the first half of the deglaciation (until around 133 ka), suggesting an increase in local surface salinity at this time. A few rapid millennial-scale oscillations were recorded between 133 and 130 ka (up to 15‰ change), roughly in accordance with the timing of the foraminiferal-based $\delta^{18}O_{sw}$ record. After reaching the highest values at around 130–129 ka, the δD_{local} record showed a sharp decrease of ~21‰, in coincidence with the observed changes in the $\delta^{18}O_{sw}$ record during the late deglaciation (Figure 2d).

5. Discussion

5.1. Primary Production in the EEP During the Penultimate Deglaciation

At ODP Site 1240, the phytoplankton community responded to the changes during the penultimate deglaciation with an increase in PP (Figures 2f and 2g). Haptophytes and diatoms production proxies showed an increase soon after the penultimate glacial maximum, steeply rising after the mid deglaciation to eventually decrease toward much lower values during the interglacial. The set of environmental conditions that favored phytoplankton growth during that period is discussed here.

The relative salinity change proxies, $\delta^{18}O_{sw}$ and δD_{local}, experienced a drastic increase toward heavier *G. ruber*-$\delta^{18}O_{sw}$ and δD_{local} isotopic values during the deglaciation (Figure 2d). Heavier $\delta^{18}O_{sw}$ values in modern EEP sea water (LeGrande & Schmidt, 2006; Pena et al., 2008) are typically found further south of the study site, toward the core of the Equatorial Pacific Cold Tongue, and also at the EUC depth domain, which both correspond to saltier water masses. This suggests that changes recorded by *G. ruber*-$\delta^{18}O_{sw}$ and δD_{local} could have been caused by an increase of the equatorial upwelling, bringing more saline EUC waters to the surface, and/or a northward shift of the EF. This interpretation is in agreement with data from the deep-thermocline dwelling foraminifera *N. dutertrei* at the same site and covering the last 275 kyr, which were linked to episodes of precession minima that accentuated the seasonal asymmetry at the equator and,

eventually, favored the occurrence of more intense and/or frequent La Niña-like conditions during deglaciations (Pena et al., 2008).

Together with an intensification of the equatorial upwelling system during the deglaciation, the significant increase in the concentration of the diatom proxies, $C_{28} + C_{30}$ 1,14-diols and brassicasterol, occurred roughly at the same time of a negative excursion of the $\delta^{13}C$ record measured on the deep-thermocline dwelling foraminifera *N. dutertrei* from the same ODP Site 1240 (previously published by Pena et al., 2008). Similar negative excursions were observed at the study site during the last three glacial terminations (Pena et al., 2008) and also in other $\delta^{13}C$ tropical and Southern Hemisphere subtropical records (Ninnemann & Charles, 1997; Shackleton et al., 1983; Spero & Lea, 2002). This has been attributed to the resumption of the Southern Ocean upwelling system during glacial terminations (e.g., Anderson et al., 2009) and the advection of low $\delta^{13}C$ waters into the SAMW source region and subsequent transport to the tropical thermocline through the EUC (Bostock et al., 2004, 2010; Pena et al., 2008, 2013; Rippert et al., 2017; Spero & Lea, 2002). The renewed upwelling during terminations also brought nutrient-rich waters to the low latitudes (Sarmiento et al., 2004). In this study, indications for the key influence of nutrient-rich Southern Ocean-sourced waters come also from the fact that all three phytoplankton productivity proxies started to increase soon after 140 ka, when *N. dutertrei*-$\delta^{13}C$ values started to decrease, and peaked between ~133 and ~127 ka, when *N. dutertrei*-$\delta^{13}C$ recorded the lowest values of the study period, suggesting maximum nutrients arrival by that time. That potential nutrient maximum arrival seemed to have a more significant impact in diatoms. As already mentioned, at that time, the relative contribution of diatoms to haptophytes increased, pointing toward a significant input of silicic acid, transported within the EUC and upwelled from the tropical thermocline to the surface, as already found for the last deglaciation (Calvo et al., 2011). Also, biogenic opal fluxes from the nearby core V19-30 (Hayes et al., 2011), with all due caution given the age uncertainties of the different age models, showed that silicified organisms responded positively to that potential input increase of silicic acid around the period of study (Figure 2g).

A second mechanism that would have significantly contributed to the observed increase in PP is the input of eolian dust as a source of iron. Our results on C_{29} *n*-alkane concentration suggest that high amounts of continental material arrived to the EEP through atmospheric deposition during the deglaciation (Figure 2f). Support for our results comes from ^{232}Th fluxes from the nearby ODP 849 core (Winckler et al., 2008). Although time resolution is low, maximum dust inputs seemed to also be recorded during the deglaciation. Different mechanisms could favor dust inputs: increased aridity in the source area, a more intense wind field, or a different wind provenance transporting material from a dustier source region. Previous studies point toward a combination of various factors being responsible for the increase in eolian dust input recorded at ODP Site 1240 during the penultimate deglaciation. On one hand, some studies found evidences of stronger southeasterly trade winds (Xie & Marcantonio, 2012) and more La Niña-like conditions (Pena et al., 2008) during the penultimate deglaciation, which would have favored the increase of eolian dust input to the study site. On the other hand, southern migrations of the South Westerlies belt during terminations could have also affected the main EEP dust source (western South America), supplying dust from a more southern source, which likely became dustier as the mountain glaciers were retreating (Pichat et al., 2014).

The hypothesis that iron fertilization from dust had a relevant role in the enhancement of EEP PP is, however, a matter of debate (Jacobel et al., 2019; Loveley et al., 2017; Marcantonio et al., 2019; Winckler et al., 2016). Studies carried out along the equator, from west of the Galapagos Islands to the Central Pacific, suggested that the most important source of iron was the upwelled waters of the EUC, since it was estimated that the amount of iron arriving through eolian dust to this region was up to two orders of magnitude less than the iron supplied by the EUC, and no correspondence was found between productivity and dust proxies (Costa et al., 2016; Winckler et al., 2016). However, other studies, mainly focused in the EEP, suggest a relevant role of continental dust as a significant source of iron (Loveley et al., 2017; Marcantonio et al., 2019; S. S. Kienast et al., 2013). Indeed, in a recent review of PP reconstructions, the EEP region east of the Galapagos Islands (where our study site is located) showed the highest variability and major discrepancies with the dominant PP trends of the rest of the Equatorial Pacific (Costa et al., 2017). In this region, the complex topography and bathymetry strongly shape wind and ocean current patterns, which make this region highly sensitive to regional forcing, such as the migrations of the ITCZ and the El Niño/Southern Oscillation (ENSO) dynamics, all together likely creating very distinct nutrient regimes

within this relatively small region. Regarding the iron supply, modern data suggest that iron concentrations arriving to the easternmost region of the EEP via the EUC are substantially less important than iron concentrations found in the EUC sections of West, Central, and East Equatorial Pacific (west of the Galapagos Islands) (Kaupp et al., 2011; Winckler et al., 2016). Eolian dust inputs to the east of the Galapagos Islands are estimated to be up to an order of magnitude higher (likely due to proximity to land) (Costa et al., 2016; Jacobel et al., 2016; S. S. Kienast et al., 2013) than those arriving to Equatorial Pacific regions west of the Galapagos Islands (Costa et al., 2016; Jacobel et al., 2016; Winckler et al., 2016). All these factors could help explain why different dust-input regimes are very likely to occur east and west of the Galapagos Islands, making our study site more prone to iron fertilization than other Equatorial Pacific regions.

5.2. The Millennial-Scale Event HE11
5.2.1. Impact of HE11 on the EEP Oceanic and Atmospheric Conditions
In this study, all PP proxies peaked between 132 and 129 ka, at a time when the isotopic *G. ruber*-δ^{18}O record registered a millennial-scale event (Pena et al., 2008; Figure 2b). This is around the time of the HE11 occurrence in the North Atlantic, shown in Figure 2a as an abrupt increase in ice rafted detritus (IRD) at ODP Site 980 (Govin et al., 2012; Irvalı et al., 2016). HEs are characterized by a collapse of the Northern Hemisphere ice sheets and the discharge of massive icebergs and freshwater into the North Atlantic (Bond & Lotti, 1995; Heinrich, 1988). These events are linked to changes in the Atlantic Meridional Overturning Circulation (AMOC) and reduction in North Atlantic Deep Water formation with important consequences on climate variability at a global scale (Alvarez-Solas et al., 2013; Barker et al., 2015, 2009; Bassis et al., 2017). For instance, during the most recent HE1 (17.5–14.5 ka, Marcott et al., 2014), an antiphase thermal state across North and South Hemispheres (seesaw effect) (Barker et al., 2009; Stenni et al., 2011) resulted in a cooling of the North Hemisphere and a warming of the South Hemisphere followed by a southward migration of the ITCZ position (Donohoe et al., 2013; Leduc et al., 2007) and the strengthening of the Southern Ocean upwelling system (Anderson et al., 2009; Siani et al., 2013).

During the penultimate deglaciation, and despite age uncertainties related to the comparison between events, our records from ODP Site 1240 seem to be affected by the global climate changes occurring during HE11. The δ^{18}O$_{sw}$ record suggests a transient freshening of surface seawaters at a time when δ^{18}O$_{sw}$ (relative salinity) had reached maximum values (Figure 2d). Although with lower time-resolution, the δD$_{local}$ record also follows the δ^{18}O$_{sw}$ trend toward a relative salinity decrease at around 130 ka. This millennial-scale structure was not so strongly reflected in the thermocline dwelling foraminifera *N. dutertrei* (same core, Pena et al., 2008), suggesting that the freshening was mostly restricted to surface seawaters. This was most likely driven by a southward displacement of the ITCZ affecting precipitation and wind patterns in this region. Evidence for recurrent southward ITCZ migrations during North Atlantic HE1 and previous HEs have been found in speleothems (Carolin et al., 2016; Cheng et al., 2013; Medina-Elizalde et al., 2017; Wang et al., 2004), as seen for the study time interval in δ^{18}O speleothem records from Borneo and Perú (Figure 2a), and marine sediments (Deplazes et al., 2013; Donohoe et al., 2013; Jacobel et al., 2016; Leduc et al., 2007; Schmidt & Spero, 2011) covering subtropical and tropical areas. Additionally, model simulations also support the idea that northeasterly trade winds would have strengthened and the ITCZ shifted to the South as a response to a shutdown of the AMOC and an increase in the high to low latitude thermal gradient in the Northern Hemisphere (Dahl et al., 2005; Vellinga & Wood, 2002; Zhang & Delworth, 2005).

Additionally, a southward displacement of the ITCZ would have also been accompanied by a warming of surface waters at the study site as a consequence of the link between the ITCZ and the EF. The ITCZ shift to the south during HE11 would have been followed by a likewise displacement of the EF causing a weakening in the upwelling and the influence of northern warm surface waters to the south. This is confirmed by a transient warming of surface seawater observed in the Mg/Ca-SST record from the same ODP Site 1240 (Pena et al., 2008). Altogether, the ITCZ and EF displacement during HE11 could explain the fresher waters (lower δ^{18}O$_{sw}$ and δD$_{local}$ values) and warmer SSTs found around the 0°N latitude in the EEP (Figure 2c, d).

5.2.2. Export Production Enhancement During HE11
Our results suggest that, during HE11, conditions in the EEP were optimal for high productivity, most likely due to the high nutrient input at this time at the study site, despite the change in EEP wind and ocean current patterns that accompanied the southward shift of the ITCZ, migrating closer to our core site. The *N. dutertrei*-δ^{13}C reached minimum values, likely pointing to a maximum influence of nutrient-rich

Southern Ocean-sourced waters (Figure 2e), and the C_{29} n-alkane record showed maximum continental eolian dust input to the study area (Figure 2f).

A major nutrient input to the EEP via the EUC could be expected at the time of HE11. HEs triggered global atmospheric and oceanic reorganizations with evidences for an additional strengthening of the already ongoing increase in Southern Ocean upwelling that started with the deglaciation (Skinner et al., 2014). For the penultimate deglaciation period, the oceanic connection with low latitudes is supported by comparing our $\delta^{13}C$ record with a high latitude benthic-$\delta^{13}C$ record from core MD97-2120 (1,210-m water depth), located east of New Zealand and bathed by AAIW (Pahnke & Zahn, 2005; Figure 2e). These two records diverge over most of the studied time interval, including the first half of the deglaciation. However, during the second half of the deglaciation, and with the caution of comparing two independently dated records, the $\delta^{13}C$ gradient between the two appeared to collapse at the approximate time of HE11 and when the highest PP values were recorded at our study site. The overlapping of the high and low latitude $\delta^{13}C$ records (Figure 2e) occurred around the time of the maximum in diatom export production in the EEP (Figure 2g), thus supporting the idea that HE11 may have triggered the maximum strengthening of the Southern Ocean upwelling system of the deglaciation which, eventually, loaded the low latitude EUC with the highest amounts of nutrients of the study period.

The PP maximum occurred when warm and low salinity surface waters were recorded at the study site (Figure 2). However, warm and low salinity surface waters in the EEP are typically associated with low productivity, as it is the case for the Eastern Pacific Warm Pool (north of the EF) or as it occurs during El Niño events (Pennington et al., 2006). The southward movement of the mean annual ITCZ position during HE11 would, a priori, bring less upwelling-favorable conditions to our site, at least during part of the year. However, the seasonal ITCZ migration would still allow for upwelling to occur during the rest of the year. In fact, the warmer and fresher sea surface conditions recorded by *G. ruber* at the study site (Figures 2c and 2d) and the higher productivity shown by phytoplankton might be partly reflecting the seasonal preferences of each organism. Sediment trap studies from the Panama Basin found that calcification and maximum production rates of *G. ruber* occurred during the non-upwelling season, that is, under warmer and less saline conditions (Fairbanks et al., 1982; Thunell et al., 1983; Thunell & Reynolds, 1984), while alkenone-based proxies better represent an annual average (M. Kienast et al., 2012). This would also explain why neither the $U_{37}^{K'}$-SST nor the δD_{local} records capture so precisely the Mg/Ca-SST warming and $\delta^{18}O_{sw}$ relative freshening during HE11 (Figure 2c, d). Therefore, the likely enhanced nutrient content of subsurface EUC waters, as suggested by the minimum in the $\delta^{13}C$ record of the thermocline foraminifera *N. dutertrei* (Pena et al., 2008), was likely a key driver for the marked increase in export production at that time, despite a diminished upwelling.

In addition to nutrients being delivered by oceanic currents, our results on C_{29} n-alkane concentration, together with ^{232}Th fluxes from ODP 849 core (Winckler et al., 2008), suggest that the highest inputs of continental material recorded at around the time of HE11 were significantly contributing to the EEP with the supply of the limiting micronutrient Fe through atmospheric deposition (Figure 2f). While dominant conditions during the penultimate deglaciation were characterized by stronger southeasterly trade winds (Pena et al., 2008) and probably drier conditions in western South America (Pichat et al., 2014), during HE11, conversely, the northeasterly trade winds intensified and the ITCZ migrated back to a more proximal location to our core site, which appeared to be causing the highest continental inputs of the study period. As mentioned, the main modern dust-supply region to our study site is the western South America, which dominates the particles flux arriving to the EEP region south of the ITCZ front (Pichat et al., 2014; Saukel et al., 2011; Xie & Marcantonio, 2012); however, the EEP region north of the ITCZ front is mainly influenced by arid regions from western and southern Mexico (Prospero & Bonatti, 1969; Saukel et al., 2011). This is so because the ITCZ acts as a barrier to cross-hemispheric dust transport (Jacobel et al., 2016; Prospero & Bonatti, 1969; Reimi & Marcantonio, 2016; Saukel et al., 2011; Xie & Marcantonio, 2012). However, with an ITCZ mean position located further south, regions from the southern Mexico could have represented an additional northern dust sources influencing the ODP Site 1240. In this regard, during more recent HEs, several studies pointed out that precipitation likely decreased over regions further south of Mexico such as northern South America and Central America, inducing drier conditions over that proximal potential dust source area to the EEP (Prospero & Bonatti, 1969; S. S. Kienast et al., 2013; Wang et al., 2004). Furthermore, model simulations

supported the prevalence of drier and dustier conditions over the study region when an AMOC shutdown was forced by mimicking the freshwater pulse of HEs in the North Atlantic (Donohoe et al., 2013; S. S. Kienast et al., 2013). Two independent δ^{18}O records measured in both Borneo and Perú cave speleothems (Figure 2a; Carolin et al., 2016; Cheng et al., 2013) showed that the ITCZ reached its southernmost position by the time HE11 was taking place in the North Atlantic, likely favoring the Central and norther South America to experience drier and therefore dustier conditions. An additional plausible mechanism to explain our recorded increase in continental input during HE11, when ODP Site 1240 was very likely located underneath the ITCZ, is an increase in wet dust deposition, as suggested from Central Equatorial Pacific records (Jacobel et al., 2016) which, together with the observation that fine eolian dust particles seem to be preferentially deposited by precipitation (Gross et al., 2016 and references therein), offer an additional or alternative possible eolian dust source which would help to explain the observed increase in eolian dust input at ODP Site 1240 during HE11 (Figure 2f). Therefore, an enhanced nutrient content of subsurface EUC waters together with an increase in dust input during HE11 likely set the optimal conditions to drive the highest increase in export primary production of the whole study period despite a diminished upwelling in the EEP.

6. Conclusions

The results of this study indicate that surface seawater conditions favorable for phytoplankton growth were established in the EEP, east of the Galapagos Islands, during the penultimate deglaciation, maximizing during HE11. At this time, an increased influence of nutrient-rich Southern Ocean-sourced waters likely favored a relief of limiting nutrients in the low-silicate, high-nutrient, low-chlorophyll region where the ODP Site 1240 is located, thus leading to a progressive increase in phytoplankton export production. The arrival of nutrients at the study site also coincided with an increase in atmospheric deposition, facilitated by the strengthening of the southeasterly trade winds, which would have favored the supply of iron to the study site. The development of HE11 in the North Atlantic triggered a southward migration of the ITCZ, the annual mean position of which may have reached as far as the equator. This shift in the ITCZ position may have caused the extension of typical Eastern Pacific Warm Pool conditions over the study site during most part of the year, also promoting enhanced dustiness in the continental areas proximal to the study region and, therefore, favoring iron fertilization. At the same time, the HE11 occurrence and its link to the reinforcement of the Southern Ocean upwelling would have brought high amounts of nutrients to the EEP through intermediate waters and the EUC. These two mechanisms would have enriched the EEP with nutrients from the atmosphere and the ocean, triggering the observed maximum in primary export production during HE11. Our results further suggest that the occurrence of HE11 likely amplified the increase in export production that was already taking place during the penultimate deglaciation.

Data Availability Statement

The new data from ODP Site 1240 core are provided in the public repository PANGAEA® (https://doi.org/10.1594/PANGAEA.916212).

References

Alvarez-Solas, J., Robinson, A., Montoya, M., & Ritz, C. (2013). Iceberg discharges of the last glacial period driven by oceanic circulation changes. *Proceedings of the National Academy of Sciences*, *110*(41), 16,350–16,354. https://doi.org/10.1073/pnas.1306622110

Anderson, R. F., Ali, S., Bradtmiller, L. I., Nielsen, S. H. H., Fleisher, M. Q., Anderson, B. E., & Burckle, L. H. (2009). Wind-driven upwelling in the Southern Ocean and the deglacial rise in atmospheric CO₂. *Science*, *323*(5920), 1443–1448. https://doi.org/10.1126/science.1167441

Badejo, A. O., Seo, I., Kim, W., Hyeong, K., & Ju, S.-J. (2017). Effect of eolian Fe-supply change on the phytoplankton productivity and community in central equatorial Pacific Ocean during the Pleistocene: A lipid biomarker approach. *Organic Geochemistry*, *112*, 170–176. https://doi.org/10.1016/j.orggeochem.2017.07.010

Barker, S., Chen, J., Gong, X., Jonkers, L., Knorr, G., & Thornalley, D. (2015). Icebergs not the trigger for North Atlantic cold events. *Nature*, *520*(7547), 333–336. https://doi.org/10.1038/nature14330

Barker, S., Diz, P., Vautravers, M. J., Pike, J., Knorr, G., Hall, I. R., & Broecker, W. S. (2009). Interhemispheric Atlantic seesaw response during the last deglaciation. *Nature*, *457*(7233), 1097–1102. https://doi.org/10.1038/nature07770

Bassis, J. N., Petersen, S. V., & Mac Cathles, L. (2017). Heinrich events triggered by ocean forcing and modulated by isostatic adjustment. *Nature*, *542*(7641), 332–334. https://doi.org/10.1038/nature21069

Bemis, B. E., Spero, H. J., Bijma, J., & Lea, D. W. (1998). Reevaluation of the oxygen isotopic composition of planktonic foraminifera: Experimental results and revised paleotemperature equations. *Paleoceanography*, *13*(2), 150–160. https://doi.org/10.1029/98PA00070

Benway, H. M., & Mix, A. C. (2004). Oxygen isotopes, upper-ocean salinity, and precipitation sources in the eastern tropical Pacific. *Earth and Planetary Science Letters*, *224*(3–4), 493–507. https://doi.org/10.1016/j.epsl.2004.05.014

Bond, G. C., & Lotti, R. (1995). Iceberg discharges into the North Atlantic on millennial time scales during the Last Glaciation. *Science*, *267*(5200), 1005–1010. https://doi.org/10.1126/science.267.5200.1005

Bostock, H. C., Opdyke, B. N., Gagan, M. K., & Fifield, L. K. (2004). Carbon isotope evidence for changes in Antarctic Intermediate Water circulation and ocean ventilation in the southwest Pacific during the last deglaciation. *Paleoceanography*, *19*, PA4013. https://doi.org/10.1029/2004PA001047

Bostock, H. C., Opdyke, B. N., & Williams, M. J. M. (2010). Characterising the intermediate depth waters of the Pacific Ocean using $\delta^{13}C$ and other geochemical tracers. *Deep Sea Research Part I: Oceanographic Research Papers*, *57*(7), 847–859. https://doi.org/10.1016/j.dsr.2010.04.005

Bradtmiller, L. I., Anderson, R. F., Fleisher, M. Q., & Burckle, L. H. (2006). Diatom productivity in the equatorial Pacific Ocean from the last glacial period to the present: A test of the silicic acid leakage hypothesis. *Paleoceanography*, *21*, PA4201. https://doi.org/10.1029/2006PA001282

Brassell, S. C. (1993). Applications of biomarkers for delineating marine paleoclimatic Fluctuations during the Pleistocene. In M. H. Engel & S. A. Mack (Eds.), *Organic Geochemistry*, *Topics in Geobiology*, (Vol. 11, pp. 699–738). Boston, MA: Springer.

Brzezinski, M. A., Baines, S. B., Balch, W. M., Beucher, C. P., Chai, F., Dugdale, R. C., et al. (2011). Co-limitation of diatoms by iron and silicic acid in the equatorial Pacific. *Deep Sea Research Part II: Topical Studies in Oceanography*, *58*(3–4), 493–511. https://doi.org/10.1016/j.dsr2.2010.08.005

Calvo, E., Pelejero, C., Logan, G. A., & De Deckker, P. (2004). Dust-induced changes in phytoplankton composition in the Tasman Sea during the last four glacial cycles. *Paleoceanography*, *19*, PA2020. https://doi.org/10.1029/2003PA000992

Calvo, E., Pelejero, C., Pena, L. D., Cacho, I., & Logan, G. A. (2011). Eastern Equatorial Pacific productivity and related-CO_2 changes since the last glacial period. *Proceedings of the National Academy of Sciences*, *108*(14), 5537–5541. https://doi.org/10.1073/pnas.1009761108

Carolin, S. A., Cobb, K. M., Lynch-Stieglitz, J., Moerman, J. W., Partin, J. W., Lejau, S., et al. (2016). Northern Borneo stalagmite records reveal West Pacific hydroclimate across MIS 5 and 6. *Earth and Planetary Science Letters*, *439*, 182–193. https://doi.org/10.1016/j.epsl.2016.01.028

Chavez, F. P. (1999). Biological and chemical response of the Equatorial Pacific Ocean to the 1997–98 El Niño. *Science*, *286*(5447), 2126–2131. https://doi.org/10.1126/science.286.5447.2126

Cheng, H., Edwards, R. L., Broecker, W. S., Denton, G. H., Kong, X., Wang, Y., et al. (2009). Ice age terminations. *Science*, *326*(5950), 248–252. https://doi.org/10.1126/science.1177840

Cheng, H., Sinha, A., Cruz, F. W., Wang, X., Edwards, R. L., D'Horta, F. M., et al. (2013). Climate change patterns in Amazonia and biodiversity. *Nature Communications*, *4*(1), 1411. https://doi.org/10.1038/ncomms2415

Conte, M. H., Sicre, M.-A., Rühlemann, C., Weber, J. C., Schulte, S., Schulz-Bull, D., & Blanz, T. (2006). Global temperature calibration of the alkenone unsaturation index ($U^{K'}_{37}$) in surface waters and comparison with surface sediments. *Geochemistry, Geophysics, Geosystems*, *7*, Q02005. https://doi.org/10.1029/2005GC001054

Costa, K. M., Jacobel, A. W., McManus, J. F., Anderson, R. F., Winckler, G., & Thiagarajan, N. (2017). Productivity patterns in the equatorial Pacific over the last 30,000 years. *Global Biogeochemical Cycles*, *31*, 850–865. https://doi.org/10.1002/2016GB005579

Costa, K. M., McManus, J. F., Anderson, R. F., Ren, H., Sigman, D. M., Winckler, G., et al. (2016). No iron fertilization in the equatorial Pacific Ocean during the last ice age. *Nature*, *529*(7587), 519–522. https://doi.org/10.1038/nature16453

Dahl, K. A., Broccoli, A. J., & Stouffer, R. J. (2005). Assessing the role of North Atlantic freshwater forcing in millennial scale climate variability: A tropical Atlantic perspective. *Climate Dynamics*, *24*(4), 325–346. https://doi.org/10.1007/s00382-004-0499-5

Deplazes, G., Lückge, A., Peterson, L. C., Timmermann, A., Hamann, Y., Hughen, K. A., et al. (2013). Links between tropical rainfall and North Atlantic climate during the last glacial period. *Nature Geoscience*, *6*(3), 213–217. https://doi.org/10.1038/ngeo1712

Donohoe, A., Marshall, J., Ferreira, D., & Mcgee, D. (2013). The relationship between ITCZ location and cross-equatorial atmospheric heat transport: From the seasonal cycle to the Last Glacial Maximum. *Journal of Climate*, *26*(11), 3597–3618. https://doi.org/10.1175/JCLI-D-12-00467.1

Dubois, N., Kienast, M., Kienast, S. S., Calvert, S. E., François, R., & Anderson, R. F. (2010). Sedimentary opal records in the eastern equatorial Pacific: It is not all about leakage. *Global Biogeochemical Cycles*, *24*, GB4020. https://doi.org/10.1029/2010GB003821

Dubois, N., Kienast, M., Kienast, S. S., Normandeau, C., Calvert, S. E., Herbert, T. D., & Mix, A. (2011). Millennial-scale variations in hydrography and biogeochemistry in the Eastern Equatorial Pacific over the last 100 kyr. *Quaternary Science Reviews*, *30*(1–2), 210–223. https://doi.org/10.1016/j.quascirev.2010.10.012

Dubois, N., Kienast, M., Kienast, S. S., & Timmermann, A. (2014). Millennial-scale Atlantic/East Pacific sea surface temperature linkages during the last 100,000 years. *Earth and Planetary Science Letters*, *396*, 134–142. https://doi.org/10.1016/j.epsl.2014.04.008

Dugdale, R. C., Wilkerson, F. P., & Minas, H. J. (1995). The role of a silicate pump in driving new production. *Deep Sea Research Part I: Oceanographic Research Papers*, *42*(5), 697–719. https://doi.org/10.1016/0967-0637(95)00015-X

Eglinton, G., & Hamilton, R. J. (1967). Leaf epicuticular waxes. *Science*, *156*(3780), 1322–1335. https://doi.org/10.1126/science.156.3780.1322

Eglinton, T. I., & Eglinton, G. (2008). Molecular proxies for paleoclimatology. *Earth and Planetary Science Letters*, *275*(1–2), 1–16. https://doi.org/10.1016/j.epsl.2008.07.012

Englebrecht, A. C., & Sachs, J. P. (2005). Determination of sediment provenance at drift sites using hydrogen isotopes and unsaturation ratios in alkenones. *Geochimica et Cosmochimica Acta*, *69*(17), 4253–4265. https://doi.org/10.1016/j.gca.2005.04.011

Fairbanks, R. G., Sverdlove, M., Free, R., Wiebe, P. H., & Bé, A. W. H. (1982). Vertical distribution and isotopic fractionation of living planktonic foraminifera from the Panama Basin. *Nature*, *298*(5877), 841–844. https://doi.org/10.1038/298841a0

Fiedler, P. C., Philbrick, V., & Chavez, F. P. (1991). Oceanic upwelling and productivity in the eastern tropical Pacific. *Limnology and Oceanography*, *36*(8), 1834–1850. https://doi.org/10.4319/lo.1991.36.8.1834

Fiedler, P. C., & Talley, L. D. (2006). Hydrography of the eastern tropical Pacific: A review. *Progress in Oceanography*, *69*(2–4), 143–180. https://doi.org/10.1016/j.pocean.2006.03.008

Gagosian, R. B., Peltzer, E. T., & Merrill, J. T. (1987). Long-range transport of terrestrially derived lipids in aerosols from the south Pacific. *Nature*, *325*(6107), 800–803. https://doi.org/10.1038/325800a0

Garcia, H. E., Locarnini, R. A., Boyer, T. P., Antonov, J. I., Baranova, O. K., Zweng, M. M., et al. (2014). World Ocean Atlas 2013, Volume 4: Dissolved Inorganic Nutrients (phosphate, nitrate, silicate). In S. Levitus (Ed.) & A. Mishonov (Technical Ed.), *NOAA Atlas NESDIS* (Vol. 76, 25 pp.).

Gat, J. R. (1996). Oxygen and hydrogen isotopes in the hydrologic cycle. *Annual Review of Earth and Planetary Sciences*, *24*(1), 225–262. https://doi.org/10.1146/annurev.earth.24.1.225

Gómez, F., Claustre, H., Raimbault, P., & Souissi, S. (2007). Two high-nutrient low-chlorophyll phytoplankton assemblages: The tropical central Pacific and the offshore Perú-Chile Current. *Biogeosciences*, *4*(6), 1101–1113. https://doi.org/10.5194/bg-4-1101-2007

Gould, J., Kienast, M., Dowd, M., & Schefuß, E. (2019). An open-ocean assessment of alkenone δD as a paleo-salinity proxy. *Geochimica et Cosmochimica Acta*, *246*, 478–497. https://doi.org/10.1016/j.gca.2018.12.004

Govin, A., Braconnot, P., Capron, E., Cortijo, E., Duplessy, J.-C., Jansen, E., et al. (2012). Persistent influence of ice sheet melting on high northern latitude climate during the early Last Interglacial. *Climate of the Past*, *8*(2), 483–507. https://doi.org/10.5194/cp-8-483-2012

Graham, N. E., & White, W. B. (1988). The El Niño cycle: A natural oscillator of the Pacific ocean-atmosphere system. *Science*, *240*(4857), 1293–1302. https://doi.org/10.1126/science.240.4857.1293

Gross, A., Turner, B. L., Goren, T., Berry, A., & Angert, A. (2016). Tracing the sources of atmospheric phosphorus deposition to a tropical rain forest in Panama using stable oxygen isotopes. *Environmental Science & Technology*, *50*(3), 1147–1156. https://doi.org/10.1021/acs.est.5b04936

Hayes, C. T., Anderson, R. F., & Fleisher, M. Q. (2011). Opal accumulation rates in the equatorial Pacific and mechanisms of deglaciation. *Paleoceanography*, *26*, PA1207. https://doi.org/10.1029/2010PA002008

Heinrich, H. (1988). Origin and consequences of cyclic ice rafting in the Northeast Atlantic Ocean during the past 130,000 years. *Quaternary Research*, *29*(2), 142–152. https://doi.org/10.1016/0033-5894(88)90057-9

Irvalı, N., Ninnemann, U. S., Kleiven, H. K. F., Galaasen, E. V., Morley, A., & Rosenthal, Y. (2016). Evidence for regional cooling, frontal advances, and East Greenland Ice Sheet changes during the demise of the last interglacial. *Quaternary Science Reviews*, *150*, 184–199. https://doi.org/10.1016/j.quascirev.2016.08.029

Jacobel, A. W., Anderson, R. F., Winckler, G., Costa, K. M., Gottschalk, J., Middleton, J. L., et al. (2019). No evidence for equatorial Pacific dust fertilization. *Nature Geoscience*, *12*(3), 154–155. https://doi.org/10.1038/s41561-019-0304-z

Jacobel, A. W., McManus, J. F., Anderson, R. F., & Winckler, G. (2016). Large deglacial shifts of the Pacific Intertropical Convergence Zone. *Nature Communications*, *7*, 10449. https://doi.org/10.1038/ncomms10449

Kasper, S., van der Meer, M. T. J., Mets, A., Zahn, R., Sinninghe Damsté, J. S., & Schouten, S. (2014). Salinity changes in the Agulhas leakage area recorded by stable hydrogen isotopes of C_{37} alkenones during Termination I and II. *Climate of the Past*, *10*(1), 251–260. https://doi.org/10.5194/cp-10-251-2014

Kaupp, L. J., Measures, C. I., Selph, K. E., & Mackenzie, F. T. (2011). The distribution of dissolved Fe and Al in the upper waters of the Eastern Equatorial Pacific. *Deep Sea Research Part II: Topical Studies in Oceanography*, *58*(3–4), 296–310. https://doi.org/10.1016/j.dsr2.2010.08.009

Kessler, W. S. (2006). The circulation of the eastern tropical Pacific: A review. *Progress in Oceanography*, *69*(2–4), 181–217. https://doi.org/10.1016/j.pocean.2006.03.009

Kienast, M., Kienast, S. S., Calvert, S. E., Eglinton, T. I., Mollenhauer, G., François, R., & Mix, A. C. (2006). Eastern Pacific cooling and Atlantic overturning circulation during the last deglaciation. *Nature*, *443*(7113), 846–849. https://doi.org/10.1038/nature05222

Kienast, M., MacIntyre, G., Dubois, N., Higginson, S., Normandeau, C., Chazen, C., & Herbert, T. D. (2012). Alkenone unsaturation in surface sediments from the eastern equatorial Pacific: Implications for SST reconstructions. *Paleoceanography*, *27*, PA1210. https://doi.org/10.1029/2011PA002254

Kienast, S. S., Friedrich, T., Dubois, N., Hill, P. S., Timmermann, A., Mix, A. C., & Kienast, M. (2013). Near collapse of the meridional SST gradient in the eastern equatorial Pacific during Heinrich Stadial 1. *Paleoceanography*, *28*, 663–674. https://doi.org/10.1002/2013PA002499

Kienast, S. S., Kienast, M., Mix, A. C., Calvert, S. E., & François, R. (2007). Thorium-230 normalized particle flux and sediment focusing in the Panama Basin region during the last 30,000 years. *Paleoceanography*, *22*, PA2213. https://doi.org/10.1029/2006PA001357

Lamy, F., Gersonde, R., Winckler, G., Esper, O., Jaeschke, A., Kuhn, G., et al. (2014). Increased dust deposition in the Pacific Southern Ocean during glacial periods. *Science*, *343*(6169), 403–407. https://doi.org/10.1126/science.1245424

Leduc, G., Vidal, L., Tachikawa, K., & Bard, E. (2010). Changes in Eastern Pacific ocean ventilation at intermediate depth over the last 150 kyr BP. *Earth and Planetary Science Letters*, *298*(1–2), 217–228. https://doi.org/10.1016/j.epsl.2010.08.002

Leduc, G., Vidal, L., Tachikawa, K., Rostek, F., Sonzogni, C., Beaufort, L., & Bard, E. (2007). Moisture transport across Central America as a positive feedback on abrupt climatic changes. *Nature*, *445*(7130), 908–911. https://doi.org/10.1038/nature05578

Legates, D. R., & Willmott, C. J. (1990). Mean seasonal and spatial variability in gauge-corrected, global precipitation. *International Journal of Climatology*, *10*(2), 111–127. https://doi.org/10.1002/joc.3370100202

LeGrande, A. N., & Schmidt, G. A. (2006). Global gridded data set of the oxygen isotopic composition in seawater. *Geophysical Research Letters*, *33*, L12604. https://doi.org/10.1029/2006GL026011

Lisiecki, L. E., & Raymo, M. E. (2005). A Pliocene–Pleistocene stack of 57 globally distributed benthic $\delta^{18}O$ records. *Paleoceanography*, *20*, PA1003. https://doi.org/10.1029/2004PA001071

Locarnini, R. A., Mishonov, A. V., Antonov, J. I., Boyer, T. P., Garcia, H. E., Baranova, O. K., et al. (2013). World Ocean Atlas 2013, Volume 1: Temperature. In S. Levitus (Ed.) & A. Mishonov (Technical Ed.), *NOAA Atlas NESDIS* (Vol. 73, 40 pp.).

López-Otálvaro, G.-E., Flores, J., Sierro, F. J., & Cacho, I. (2008). Variations in coccolithophorid production in the Eastern Equatorial Pacific at ODP Site 1240 over the last seven glacial-interglacial cycles. *Marine Micropaleontology*, *69*(1), 52–69. https://doi.org/10.1016/j.marmicro.2007.11.009

Loubere, P. (2000). Marine control of biological production in the eastern equatorial Pacific Ocean. *Nature*, *406*(6795), 497–500. https://doi.org/10.1038/35020041

Loveley, M. R., Marcantonio, F., Wisler, M. M., Hertzberg, J. E., Schmidt, M. W., & Lyle, M. (2017). Millennial-scale iron fertilization of the eastern equatorial Pacific over the past 100,000 years. *Nature Geoscience*, *10*(10), 760–764. https://doi.org/10.1038/ngeo3024

Lukas, R. (1986). The termination of the Equatorial Undercurrent in the eastern Pacific. *Progress in Oceanography*, *16*(2), 63–90. https://doi.org/10.1016/0079-6611(86)90007-8

M'boule, D., Chivall, D., Sinke-Schoen, D., Sinninghe Damsté, J. S., Schouten, S., & van der Meer, M. T. J. (2014). Salinity dependent hydrogen isotope fractionation in alkenones produced by coastal and open ocean haptophyte algae. *Geochimica et Cosmochimica Acta*, *130*, 126–135. https://doi.org/10.1016/j.gca.2014.01.029

Marcantonio, F., Loveley, M. R., Schmidt, M. W., & Hertzberg, J. E. (2019). Reply to: No evidence for equatorial Pacific dust fertilization. *Nature Geoscience*, *12*(3), 156–156. https://doi.org/10.1038/s41561-019-0305-y

Marcott, S. A., Bauska, T. K., Buizert, C., Steig, E. J., Rosen, J. L., Cuffey, K. M., et al. (2014). Centennial-scale changes in the global carbon cycle during the last deglaciation. *Nature*, *514*(7524), 616–619. https://doi.org/10.1038/nature13799

Martínez-Garcia, A., Rosell-Melé, A., Geibert, W., Gersonde, R., Masqué, P., Gaspari, V., & Barbante, C. (2009). Links between iron supply, marine productivity, sea surface temperature, and CO_2 over the last 1.1 Ma. *Paleoceanography*, *24*, PA1207. https://doi.org/10.1029/2008PA001657

Martínez-Garcia, A., Rosell-Melé, A., Jaccard, S. L., Geibert, W., Sigman, D. M., & Haug, G. H. (2011). Southern Ocean dust-climate coupling over the past four million years. *Nature*, *476*(7360), 312–315. https://doi.org/10.1038/nature10310

Medina-Elizalde, M., Burns, S. J., Polanco-Martinez, J., Lases-Hernández, F., Bradley, R., Wang, H.-C., & Shen, C.-C. (2017). Synchronous precipitation reduction in the American Tropics associated with Heinrich 2. *Scientific Reports*, *7*(1), 11216. https://doi.org/10.1038/s41598-017-11742-8

Müller, P. J., Kirst, G., Ruhland, G., von Storch, I., & Rosell-Melé, A. (1998). Calibration of the alkenone paleotemperature index $U^{K'}_{37}$ based on core-tops from the eastern South Atlantic and the global ocean (60°N-60°S). *Geochimica et Cosmochimica Acta*, *62*(10), 1757–1772. https://doi.org/10.1016/S0016-7037(98)00097-0

Ninnemann, U. S., & Charles, C. D. (1997). Regional differences in Quaternary subantarctic nutrient cycling: Link to intermediate and deep water ventilation. *Paleoceanography*, *12*(4), 560–567. https://doi.org/10.1029/97PA01032

Pahnke, K., Sachs, J. P., Keigwin, L., Timmermann, A., & Xie, S.-P. (2007). Eastern tropical Pacific hydrologic changes during the past 27,000 years from D/H ratios in alkenones. *Paleoceanography*, *22*, PA4214. https://doi.org/10.1029/2007PA001468

Pahnke, K., & Zahn, R. (2005). Southern Hemisphere water mass conversion linked with North Atlantic climate variability. *Science*, *307*(5716), 1741–1746. https://doi.org/10.1126/science.1102163

Pelejero, C., Grimalt, J. O., & Cacho, I. (1997). Aplicaciones de los biomarcadores moleculares en estudios paleoclimáticos: las alquenonas y el índice U^{K}_{37}. *Thalassas*, *13*, 49–58.

Pena, L. D., Cacho, I., Ferretti, P., & Hall, M. A. (2008). El Niño-Southern Oscillation-like variability during glacial terminations and interlatitudinal teleconnections. *Paleoceanography*, *23*, PA3101. https://doi.org/10.1029/2008PA001620

Pena, L. D., Goldstein, S. L., Hemming, S. R., Jones, K. M., Calvo, E., Pelejero, C., & Cacho, I. (2013). Rapid changes in meridional advection of Southern Ocean intermediate waters to the tropical Pacific during the last 30 kyr. *Earth and Planetary Science Letters*, *368*, 20–32. https://doi.org/10.1016/j.epsl.2013.02.028

Pennington, J. T., Mahoney, K. L., Kuwahara, V. S., Kolber, D. D., Calienes, R., & Chavez, F. P. (2006). Primary production in the eastern tropical Pacific: A review. *Progress in Oceanography*, *69*(2–4), 285–317. https://doi.org/10.1016/j.pocean.2006.03.012

Philander, S. G. H., Gu, D., Lambert, G., Li, T., Halpern, D., Lau, N.-C., & Pacanowski, R. C. (1996). Why the ITCZ is mostly north of the equator. *Journal of Climate*, *9*(12), 2958–2972. https://doi.org/10.1175/1520-0442(1996)009<2958:WTIIMN>2.0.CO;2

Pichat, S., Abouchami, W., & Galer, S. J. G. (2014). Lead isotopes in the Eastern Equatorial Pacific record Quaternary migration of the South Westerlies. *Earth and Planetary Science Letters*, *388*, 293–305. https://doi.org/10.1016/j.epsl.2013.11.035

Povea, P., Cacho, I., Moreno, A., Pena, L. D., Menéndez, M., Calvo, E., et al. (2016). Atmosphere-ocean linkages in the eastern equatorial Pacific over the early Pleistocene. *Paleoceanography*, *31*, 522–538. https://doi.org/10.1002/2015PA002883

Prahl, F. G., & Wakeham, S. G. (1987). Calibration of unsaturation patterns in long-chain ketone compositions for palaeotemperature assessment. *Nature*, *330*(6146), 367–369. https://doi.org/10.1038/330367a0

Prospero, J. M., & Bonatti, E. (1969). Continental dust in the atmosphere of the Eastern Equatorial Pacific. *Journal of Geophysical Research*, *74*(13), 3362–3371. https://doi.org/10.1029/JC074i013p03362

Rampen, S. W., Abbas, B. A., Schouten, S., & Sinninghe Damsté, J. S. (2010). A comprehensive study of sterols in marine diatoms (Bacillariophyta): Implications for their use as tracers for diatom productivity. *Limnology and Oceanography*, *55*(1), 91–105. https://doi.org/10.4319/lo.2010.55.1.0091

Rampen, S. W., Schouten, S., Koning, E., Brummer, G. J. A., & Sinninghe Damsté, J. S. (2008). A 90 kyr upwelling record from the northwestern Indian Ocean using a novel long-chain diol index. *Earth and Planetary Science Letters*, *276*(1–2), 207–213. https://doi.org/10.1016/j.epsl.2008.09.022

Rampen, S. W., Schouten, S., & Sinninghe Damsté, J. S. (2011). Occurrence of long chain 1,14-diols in *Apedinella radians*. *Organic Geochemistry*, *42*(5), 572–574. https://doi.org/10.1016/j.orggeochem.2011.03.009

Reimi, M. A., & Marcantonio, F. (2016). Constraints on the magnitude of the deglacial migration of the ITCZ in the Central Equatorial Pacific Ocean. *Earth and Planetary Science Letters*, *453*, 1–8. https://doi.org/10.1016/j.epsl.2016.07.058

Rincón-Martínez, D., Steph, S., Lamy, F., Mix, A., & Tiedemann, R. (2011). Tracking the equatorial front in the eastern equatorial Pacific Ocean by the isotopic and faunal composition of planktonic foraminifera. *Marine Micropaleontology*, *79*(1–2), 24–40. https://doi.org/10.1016/j.marmicro.2011.01.001

Rippert, N., Max, L., Mackensen, A., Cacho, I., Povea, P., & Tiedemann, R. (2017). Alternating influence of northern versus southern-sourced water masses on the Equatorial Pacific subthermocline during the past 240 ka. *Paleoceanography*, *32*, 1256–1274. https://doi.org/10.1002/2017PA003133

Robinson, R. S., Martinez, P., Pena, L. D., & Cacho, I. (2009). Nitrogen isotopic evidence for deglacial changes in nutrient supply in the eastern equatorial Pacific. *Paleoceanography*, *24*, PA4213. https://doi.org/10.1029/2008PA001702

Rozanski, K., Araguás-Araguás, L., & Gonfiantini, R. (1993). Isotopic patterns in modern global precipitation. In P. K. Swart, K. C. Lohmann, J. Mckenzie, & S. Savin (Eds.), *Climate Change in Continental Isotopic Records*, *Geophysical Monograph Series* (Vol. 78, 1–36). Washington, DC: American Geophysical Union. https://doi.org/10.1029/GM078p0001

Sarmiento, J. L., Gruber, N., Brzezinski, M. A., & Dunne, J. P. (2004). High-latitude controls of thermocline nutrients and low latitude biological productivity. *Nature*, *427*(6969), 56–60. https://doi.org/10.1038/nature02127

Saukel, C., Lamy, F., Stuut, J. W., Tiedemann, R., & Vogt, C. (2011). Distribution and provenance of wind-blown SE Pacific surface sediments. *Marine Geology*, *280*(1–4), 130–142. https://doi.org/10.1016/j.margeo.2010.12.006

Schmidt, M. W., & Spero, H. J. (2011). Meridional shifts in the marine ITCZ and the tropical hydrologic cycle over the last three glacial cycles. *Paleoceanography*, *26*, PA1206. https://doi.org/10.1029/2010PA001976

Schneider, T., Bischoff, T., & Haug, G. H. (2014). Migrations and dynamics of the intertropical convergence zone. *Nature*, *513*(7516), 45–53. https://doi.org/10.1038/nature13636

Schouten, S., Ossebaar, J., Schreiber, K., Kienhuis, M. V. M., Langer, G., Benthien, A., & Bijma, J. (2006). The effect of temperature, salinity and growth rate on the stable hydrogen isotopic composition of long chain alkenones produced by *Emiliania huxleyi* and *Gephyrocapsa oceanica*. *Biogeosciences*, *3*(1), 113–119. https://doi.org/10.5194/bg-3-113-2006

Shackleton, N. J., Hall, M. A., Line, J., & Shuxi, C. (1983). Carbon isotope data in core V19-30 confirm reduced carbon dioxide concentration in the ice age atmosphere. *Nature*, *306*(5941), 319–322. https://doi.org/10.1038/306319a0

Shakun, J. D., Clark, P. U., He, F., Marcott, S. A., Mix, A. C., Liu, Z., et al. (2012). Global warming preceded by increasing carbon dioxide concentrations during the last deglaciation. *Nature*, *484*(7392), 49–54. https://doi.org/10.1038/nature10915

Siani, G., Michel, E., De Pol-Holz, R., DeVries, T., Lamy, F., Carel, M., et al. (2013). Carbon isotope records reveal precise timing of enhanced Southern Ocean upwelling during the last deglaciation. *Nature Communications*, *4*(1), 2758. https://doi.org/10.1038/ncomms3758

Sigman, D. M., & Boyle, E. A. (2000). Glacial/interglacial variations in atmospheric carbon dioxide. *Nature*, *407*(6806), 859–869. https://doi.org/10.1038/35038000

Singh, A. K., Marcantonio, F., & Lyle, M. (2011). Sediment focusing in the Panama Basin, Eastern Equatorial Pacific Ocean. *Earth and Planetary Science Letters*, *309*(1–2), 33–44. https://doi.org/10.1016/j.epsl.2011.06.020

Sinninghe Damsté, J. S., Rampen, S., Irene, W., Rijpstra, C., Abbas, B., Muyzer, G., & Schouten, S. (2003). A diatomaceous origin for long-chain diols and mid-chain hydroxy methyl alkanoates widely occurring in quaternary marine sediments: indicators for high-nutrient conditions. *Geochimica et Cosmochimica Acta*, *67*(7), 1339–1348. https://doi.org/10.1016/S0016-7037(02)01225-5

Skinner, L. C., Waelbroeck, C., Scrivner, A. E., & Fallon, S. J. (2014). Radiocarbon evidence for alternating northern and southern sources of ventilation of the deep Atlantic carbon pool during the last deglaciation. *Proceedings of the National Academy of Sciences*, *111*(15), 5480–5484. https://doi.org/10.1073/pnas.1400668111

Spero, H. J., & Lea, D. W. (2002). The cause of carbon isotope minimum events on glacial terminations. *Science*, *296*(5567), 522–525. https://doi.org/10.1126/science.1069401

Stenni, B., Buiron, D., Frezzotti, M., Albani, S., Barbante, C., Bard, E., et al. (2011). Expression of the bipolar see-saw in Antarctic climate records during the last deglaciation. *Nature Geoscience*, *4*(1), 46–49. https://doi.org/10.1038/ngeo1026

Takahashi, T., Sutherland, S. C., Wanninkhof, R., Sweeney, C., Feely, R. A., Chipman, D. W., et al. (2009). Climatological mean and decadal change in surface ocean pCO_2, and net sea-air CO_2 flux over the global oceans. *Deep Sea Research Part II: Topical Studies in Oceanography*, *56*(8–10), 554–577. https://doi.org/10.1016/j.dsr2.2008.12.009

Thunell, R. C., Curry, W. B., & Honjo, S. (1983). Seasonal variation in the flux of planktonic foraminifera: Time series sediment trap results from the Panama Basin. *Earth and Planetary Science Letters*, *64*(1), 44–55. https://doi.org/10.1016/0012-821X(83)90051-1

Thunell, R. C., & Reynolds, L. A. (1984). Sedimentation of planktonic foraminifera: Seasonal changes in species flux in the Panama Basin. *Micropaleontology*, *30*(3), 243. https://doi.org/10.2307/1485688

Timmermann, A., Okumura, Y., An, S.-I., Clement, A., Dong, B., Guilyardi, E., et al. (2007). The influence of a weakening of the Atlantic Meridional Overturning Circulation on ENSO. *Journal of Climate*, *20*(19), 4899–4919. https://doi.org/10.1175/JCLI4283.1

Toggweiler, J. R., Dixon, K., & Broecker, W. S. (1991). The Peru upwelling and the ventilation of the south Pacific thermocline. *Journal of Geophysical Research*, *96*(C11), 20467. https://doi.org/10.1029/91JC02063

Tsuchiya, M. (1981). The origin of the Pacific Equatorial 13°C water. *Journal of Physical Oceanography*, *11*(6), 794–812. https://doi.org/10.1175/1520-0485(1981)011<0794:TOOTPE>2.0.CO;2

Tsuchiya, M., Lukas, R., Fine, R. A., Firing, E., & Lindstrom, E. (1989). Source waters of the Pacific Equatorial Undercurrent. *Progress in Oceanography*, *23*(2), 101–147. https://doi.org/10.1016/0079-6611(89)90012-8

van der Meer, M. T. J., Benthien, A., Bijma, J., Schouten, S., & Sinninghe Damsté, J. S. (2013). Alkenone distribution impacts the hydrogen isotopic composition of the $C_{37:2}$ and $C_{37:3}$ alkan-2-ones in *Emiliania huxleyi*. *Geochimica et Cosmochimica Acta*, *111*, 162–166. https://doi.org/10.1016/j.gca.2012.10.041

Vellinga, M., & Wood, R. A. (2002). Global climatic impacts of a collapse of the Atlantic Thermohaline Circulation. *Climatic Change*, *54*(3), 251–267. https://doi.org/10.1023/A:1016168827653

Villanueva, J., Calvo, E., Pelejero, C., Grimalt, J. O., Boelaert, A., & Labeyrie, L. (2001). A latitudinal productivity band in the central North Atlantic over the last 270 kyr: An alkenone perspective. *Paleoceanography*, *16*(6), 617–626. https://doi.org/10.1029/2000PA000543

Villanueva, J., Pelejero, C., & Grimalt, J. O. (1997). Clean-up procedures for the unbiased estimation of C37 alkenone sea surface temperatures and terrigenous n-alkane inputs in paleoceanography. *Journal of Chromatography A*, *757*(1–2), 145–151. https://doi.org/10.1016/S0021-9673(96)00669-3

Volkman, J. K. (2003). Sterols in microorganisms. *Applied Microbiology and Biotechnology*, *60*(5), 495–506. https://doi.org/10.1007/s00253-002-1172-8

Volkman, J. K., Eglinton, G., Corner, E. D. S., & Forsberg, T. E. V. (1980). Long-chain alkenes and alkenones in the marine coccolithophorid *Emiliania huxleyi*. *Phytochemistry*, *19*(12), 2619–2622. https://doi.org/10.1016/S0031-9422(00)83930-8

Volkman, J. K., Smith, D. J., Eglinton, G., Forsberg, T. E. V., & Corner, E. D. S. (1981). Sterol and fatty acid composition of four marine haptophycean algae. *Journal of the Marine Biological Association of the United Kingdom*, *61*(02), 509. https://doi.org/10.1017/S0025315400047111

Waelbroeck, C., Labeyrie, L., Michel, E., Duplessy, J. C., McManus, J. F., Lambeck, K., et al. (2002). Sea-level and deep water temperature changes derived from benthic foraminifera isotopic records. *Quaternary Science Reviews*, *21*(1–3), 295–305. https://doi.org/10.1016/S0277-3791(01)00101-9

Waliser, D. E., & Gautier, C. (1993). A satellite-derived climatology of the ITCZ. *Journal of Climate*, *6*(11), 2162–2174. https://doi.org/10.1175/1520-0442(1993)006<2162:ASDCOT>2.0.CO;2

Wang, X., Auler, A. S., Edwards, R. L., Cheng, H., Cristalli, P. S., Smart, P. L., et al. (2004). Wet periods in northeastern Brazil over the past 210 kyr linked to distant climate anomalies. *Nature*, *432*(7018), 740–743. https://doi.org/10.1038/nature03067

Watkins, J. M., Mix, A. C., & Wilson, J. (1998). Living planktic foraminifera in the central tropical Pacific Ocean: Articulating the equatorial 'cold tongue' during La Niña, 1992. *Marine Micropaleontology*, *33*(3–4), 157–174. https://doi.org/10.1016/S0377-8398(97)00036-4

Weiss, G. M., de Bar, M. W., Stolwijk, D. J., Schouten, S., Sinninghe Damsté, J. S., & van der Meer, M. T. J. (2019a). Paleosensitivity of hydrogen isotope ratios of long-chain alkenones to salinity changes at the Chile margin. *Paleoceanography and Paleoclimatology*, *34*, 978–989. https://doi.org/10.1029/2019PA003591

Weiss, G. M., Schouten, S., Sinninghe Damsté, J. S., & van der Meer, M. T. J. (2019b). Constraining the application of hydrogen isotopic composition of alkenones as a salinity proxy using marine surface sediments. *Geochimica et Cosmochimica Acta*, *250*, 34–48. https://doi.org/10.1016/j.gca.2019.01.038

Werne, J. P., Hollander, D. J., Lyons, T. W., & Peterson, L. C. (2000). Climate-induced variations in productivity and planktonic ecosystem structure from the Younger Dryas to Holocene in the Cariaco Basin, Venezuela. *Paleoceanography*, *15*(1), 19–29. https://doi.org/10.1029/1998PA000354

Winckler, G., Anderson, R. F., Fleisher, M. Q., McGee, D., & Mahowald, N. (2008). Covariant glacial-interglacial dust fluxes in the Equatorial Pacific and Antarctica. *Science*, *320*(5872), 93–96. https://doi.org/10.1126/science.1150595

Winckler, G., Anderson, R. F., Jaccard, S. L., & Marcantonio, F. (2016). Ocean dynamics, not dust, have controlled equatorial Pacific productivity over the past 500,000 years. *Proceedings of the National Academy of Sciences*, *113*(22), 6119–6124. https://doi.org/10.1073/pnas.1600616113

Xie, R. C., & Marcantonio, F. (2012). Deglacial dust provenance changes in the Eastern Equatorial Pacific and implications for ITCZ movement. *Earth and Planetary Science Letters*, *317–318*, 386–395. https://doi.org/10.1016/j.epsl.2011.11.014

Zhang, R., & Delworth, T. L. (2005). Simulated tropical response to a substantial weakening of the Atlantic Thermohaline Circulation. *Journal of Climate*, *18*(12), 1853–1860. https://doi.org/10.1175/JCLI3460.1

Zweng, M. M., Reagan, J. R., Antonov, J. I., Locarnini, R. A., Mishonov, A. V., Boyer, A. V., et al. (2013). World Ocean Atlas 2013, Volume 2: Salinity. In S. Levitus (Ed.) & A. Mishonov (Technical Ed.), *NOAA Atlas NESDIS* (Vol. 79, 39 pp.).